Journal of Organometallic Chemistry 760 (2014) 48–54

Contents lists available at ScienceDirect

Journal of Organometallic Chemistry

journal homepage: www.elsevier.com/locate/jorganchem

Solution and solid state properties of Fe(III) complexes bearing *N*-ethyl-*N*-(2-aminoethyl)salicylaldiminate ligands

Paulo N. Martinho [a,*], Ana I. Vicente [a], Sara Realista [a], Marta S. Saraiva [a], Ana I. Melato [a], Paula Brandão [b], Liliana P. Ferreira [c,d], Maria de Deus Carvalho [e]

[a] CQB, Departamento de Química e Bioquímica, Faculdade de Ciências, Universidade de Lisboa, Campo Grande, 1749-016 Lisboa, Portugal
[b] Departamento de Química, CICECO, Universidade de Aveiro, 3810-193 Aveiro, Portugal
[c] CFMC, Faculdade de Ciências, Universidade de Lisboa, Campo Grande, 1749-016 Lisboa, Portugal
[d] Departamento de Física, Faculdade de Ciências e Tecnologia, Universidade de Coimbra, 3004-516 Coimbra, Portugal
[e] CCMM, Departamento de Química e Bioquímica, Faculdade de Ciências, Universidade de Lisboa, Campo Grande, 1749-016 Lisboa, Portugal

ARTICLE INFO

Article history:
Received 12 November 2013
Received in revised form
13 December 2013
Accepted 14 December 2013

Dedicated to Prof. Maria José Calhorda on the occasion of her 65th birthday

Keywords:
Spin crossover
Fe(III) complexes
Electron withdrawing groups
Evans method
Cyclic voltammetry

ABSTRACT

The effect of the phenolate ring derivatisation on the magnetic properties of Fe(III) complexes bearing *N*-ethyl-*N*-(2-aminoethyl)salicylaldiminate ligands both in solid state and solution have been investigated. Two new complexes $[Fe(3,5\text{-Br-salEen})_2]ClO_4.EtOH$ (**5**) and $[Fe(3,5\text{-Br-salEen})_2]BPh_4.DMF$ (**6**) have been synthesised. SQUID magnetometry studies on these complexes showed that while complex **5** is in the low-spin (LS) state, complex **6** displays a gradual and incomplete spin crossover (SCO) transition over the temperature measured. Solution measurements on a series of six complexes – $[Fe(salEen)_2]ClO_4$ (**1**), $[Fe(salEen)_2]BPh_4\cdot 0.5H_2O$ (**2**), $[Fe(5\text{-Br-salEen})_2]ClO_4$ (**3**), $[Fe(5\text{-Br-salEen})_2]BPh_4\cdot DMF$ (**4**), $[Fe(3,5\text{-Br-salEen})_2]ClO_4\cdot EtOH$ (**5**) and $[Fe(3,5\text{-Br-salEen})_2]BPh_4\cdot DMF$ (**6**) – were performed by UV–vis and NMR spectroscopies and cyclic voltammetry. Solution studies show that the presence of electron withdrawing groups (bromine atoms) affect the electronic density at the phenolate ring, thus influencing the ligand field strength and the separation between the t_{2g} and e_g^* energy levels. The presence of two bromide substituents at the phenolate ring has a more pronounced effect on the magnetic behaviour in solution than in the solid state, with both complexes **5** and **6** adopting preferentially the LS state. Electrochemical studies of complexes **1**–**6** reveal that the reduction of the metallic centres in the complexes with electron withdrawing groups is easier, with $E_{1/2}$ values of iron moving to more positive potentials with the number of bromide substituents at the phenolate ring.

1. Introduction

Schiff base ligands are very versatile for coordination to transition metal ions. Complexes with Schiff base ligands have been widely studied [1] and coordination to first row transition metal ions can display interesting magnetic properties, particularly SCO or spin transition (ST) [2–4]. SCO is commonly observed for octahedral metal complexes with a metal $3d^4$ to $3d^7$ electron configuration which can interchange between two electronic states, high-spin (HS) and LS, by application of an external perturbation such as temperature, pressure, light or magnetic field. SCO was first reported by Cambi and co-workers after detecting unusual magnetism in Fe(III) derivatives of various dithiocarbamates [5–7]. Later, the vision of Kahn and co-workers towards the application of SCO compounds in data processing [8] resulted in a long and impressive literature on SCO. This included the discovery of several new examples of SCO compounds [3,9–11], the explanation of different types of SCO profiles [4,12] and the modification of SCO compounds to increase cooperativity and to direct their application into materials science [13]. Scientists have developed SCO networks [14–16], frameworks [17–19], gels [20–22], liquid crystals [23–25], nanoparticles and nanocrystals [26–29], nanowires [30], thin films [31–33] and have also applied patterning techniques to fabricate SCO devices [34]. Among complexes displaying SCO, $[Fe(salEen)_2]^+$ derivatives (salEen = *N*-ethyl-*N*-(2-aminoethyl)salicylaldiminate) are known to undergo thermal SCO sensitive to unit cell contents and supramolecular packing in the crystal [35].

Hendrickson and co-workers reported the first examples of salEen derivatives SCO compounds and also reported the distinct

* Corresponding author. DQB/FCUL, Campo Grande, Ed. C8, 1749-016 Lisboa, Portugal. Tel.: +351 217500978; fax: +351 217500088.
E-mail address: pnmartinho@fc.ul.pt (P.N. Martinho).

0022-328X/$ – see front matter © 2013 Elsevier B.V. All rights reserved.
http://dx.doi.org/10.1016/j.jorganchem.2013.12.028

abrupt SCO profile for the $[Fe(3\text{-}OMe\text{-}salEen)_2]PF_6$ system [36]. This report led to a number of new SCO compounds of the type $[Fe(X\text{-}salEen)_2]Y$ (X = H, 3-OMe, 4-OMe or 5-OMe; $Y = Cl^-$, ClO_4^-, NO_3^-, PF_6^-, or BPh_4^-) [35,37] displaying a range of SCO profiles from incomplete and gradual to complete. Among salEen derivatives, it has been observed that Cl^- and NO_3^- complexes tend to stabilise the LS state, and BPh_4^- complexes adopt preferably the HS state [35,36,38]. In solution the SCO process becomes an individual molecular process and abrupt and hysteretic SCO is not expected unless self-assembly occurs and interaction is sensed by neighbouring molecules [39]. Additionally, the rigidity conferred by the solid state intermolecular lattices is not observed and the solvent and anion effect on the ligand field strength can be studied.

We have recently found that $[Fe(5\text{-}Br\text{-}salEen)_2]^+$ displays different types of SCO profiles depending on the anion used and the solvation of the unit cell [40]. We also observed that the H-bonding between the ligand and the anion is crucial and a key to promote SCO at room-temperature (RT). This work reports the effect of electron withdrawing groups on the magnetic behaviour of the metal both in solid state and solution. The ligands salEen (L_A), 5-Br-salEen (L_B) and 3,5-Br-salEen (L_C) have been chosen and their ClO_4^- and BPh_4^- Fe(III) complexes, $[Fe(X\text{-}salEen)_2]Y$ (X = H, 5-Br or 3,5-Br; Y = ClO_4^- or BPh_4^-), investigated. Solid state magnetic properties of $[Fe(3,5\text{-}Br\text{-}salEen)_2]ClO_4\cdot EtOH$ (**5**) and $[Fe(3,5\text{-}Br\text{-}salEen)_2]BPh_4\cdot DMF$ (**6**) are reported as well as redox behaviour and magnetic properties in solution at RT for $[Fe(salEen)_2]ClO_4$ (**1**), $[Fe(salEen)_2]BPh_4\cdot 0.5H_2O$ (**2**), $[Fe(5\text{-}Br\text{-}salEen)_2]ClO_4$ (**3**), $[Fe(5\text{-}Br\text{-}salEen)_2]BPh_4\cdot DMF$ (**4**), $[Fe(3,5\text{-}Br\text{-}salEen)_2]ClO_4\cdot EtOH$ (**5**) and $[Fe(3,5\text{-}Br\text{-}salEen)_2]BPh_4\cdot DMF$ (**6**).

2. Experimental

2.1. Materials and measurements

Salicylaldehyde, 5-bromosalicylaldehyde, 3,5-dibromosalicylaldehyde, iron(III) nitrate nonahydrate, iron(II) chloride, *N*-ethylethylenediamine, sodium perchlorate, sodium tetraphenylborate, tetrabutylammonium tetrafluoroborate and solvents were purchased and used without further purification. IR spectra (KBr pellets) were recorded on a Nicolet Nexus 6700 FTIR spectrophotometer. UV–vis spectra were recorded on a Shimadzu 50/60 Hz spectrometer in acetonitrile solutions. Microanalyses (C, H and N) were measured by elemental analysis service at the University of Vigo, Spain.

Magnetisation measurements as a function of temperature were performed using an SQUID magnetometer (Quantum Design MPMS). The curves were obtained at 1000 Oe for temperatures ranging from 10 to 370 K and the molar susceptibilities (χ_m) values were corrected for diamagnetism.

The Mössbauer spectra were recorded in transmission mode at RT and at 78 K using a conventional constant-acceleration spectrometer and a 50 mCi ^{57}Co source in a Rh matrix. The low temperature measurements were performed using a liquid nitrogen flow cryostat with a temperature stability of ±0.5 K. The velocity scale was calibrated using an α-Fe foil. The spectra were fitted to Lorentzian lines using the WinNormos software program, and the isomer shifts reported are relative to metallic α-Fe at RT.

Magnetic measurements of complexes **1**–**6** in solution were performed at RT by ^1H NMR using the Evans' method [41] (Bruker Avance 400 spectrometer operating at 400.14 MHz at a constant temperature of 298.15 K). The measurements were performed in NMR tubes containing the paramagnetic samples (5 mM) dissolved in CD_3CN with an inert reference of 0.03% TMS, against a reference insert tube filled with the same solvent (0.03% TMS in CD_3CN). The difference between the shifts (in Hz) given by the TMS outside and inside the insert tube were measured and the mass susceptibility (χ_g) calculated from,

$$\chi_g = \chi_0 + \frac{3000\Delta\nu}{4\pi\nu_0 CM}$$

where *C* is the concentration of the sample and *M* is the molecular weight of the paramagnetic molecule. The molar susceptibility (χ_m) of the paramagnetic species is derived from the previous expression after appropriate diamagnetic correction.

Electrochemical studies were performed using a CHI Electrochemical Analyser – 620A controlled by software. A one-compartment glass cell was used in all experiments; a platinum wire and a platinum foil (1 cm^2) were used as working and counter electrodes, respectively. A saturated calomel electrode (SCE, 0.244 V vs. SHE) was used as reference electrode. Before each experiment the working electrode was cleaned by flame-annealing in a butane–oxygen Bunsen burner until the slide attained dark red glowing. All solutions were deoxygenated directly in the electrochemical cell with a stream of N_2 for 5 min. All experiments were performed in dry acetonitrile solutions (1 mM) and tetrabutylammonium tetrafluoroborate (NBu_4BF_4, 0.1 M). For complexes **1**–**6**, ferrocene ($E_{1/2}$ = 0.420 V vs. SCE) [42] was used as internal standard.

Single X-ray crystal data for **6** were collected at 150(2) K by using a Bruker SMART APEX II diffractometer equipped with a CCD area detector and monochromated Mo-Kα radiation (λ = 0.71073 Å). The frames were integrated with the SAINT-Plus software package [43], and the intensities were corrected for polarisation and Lorentz effects. A multi-scan absorption correction was also applied with the SADABS [44]. The structure was solved by direct methods with SHELXS-2013 [45] and refined by full-matrix least-squares based on F^2 using the program SHELXL-2013 [45]. Hydrogen atoms bound to carbon and nitrogen were inserted at ideal geometric positions. ORTEP and packing diagrams were drawn with the Olex2 [46] and the Mercury software packages [47], respectively. The crystal data together with refinement details are given in Table 1. The crystal structure has been deposited with CCDC 976390.

2.2. Synthesis of compounds *1*–*4*

Compounds **1** and **2** were obtained as described in the literature [38,48]. Compounds **3** and **4** were synthesised as previously described by our group [40].

Table 1
Crystal data parameters and selected refinement details of **6**.

Empirical Formula	$C_{49}H_{53}BBr_4FeN_5O_3$
M_w	1146.26
Crystal system	Monoclinic
Space group	$P2_1/n$
a/Å	15.1177(4)
b/Å	15.6799(4)
c/Å	20.7440(5)
V/Å^3	4906.3(2)
Z	4
ρ_{calc}/mg mm^{-3}	1.52
μ/mm^{-1}	0.500
$F(000)$	2308
2θ range for data collection/°	
Index ranges	$-19 \le h \le 16$, $-20 \le k \le 20$, $-27 \le l \le 27$
Crystal size/mm	0.5 × 0.12 × 0.03
Reflections collected	65,747
Unique reflections, [R_{int}]	11,722 [0.0453]
Final $R_{indices}$	
R_1, wR_2 [$I > 2\sigma I$]	0.0346, 0.0779 [8400]
R_1, wR_2 (all data)	0.0630, 0.0917

2.3. Synthesis of compound **5** – [Fe(3,5-Br-salEen)$_2$]ClO$_4$·EtOH

To a solution of *N*-ethylethylenediamine (0.105 mL, 1 mmol) in methanol (20 mL) 3,5-dibromosalicylaldehyde (279 mg, 1 mmol) was added and left stirring for 15 min to give a yellow solution. A solution of iron(II) chloride (64 mg, 0.5 mmol) and sodium perchlorate monohydrate (70 mg, 0.5 mmol) in methanol was added to the mixture and left stirring for 1 h. The purple solution was filtered and a dark solid was obtained after slow evaporation of the solvent. The crude solid was recrystallised from an ethanol/methanol mixture (50:50) yielding a microcrystalline solid after slow evaporation of the solvent (108 mg, 13%). IR: ν_{max}/cm^{-1} 3210 (ν_{NH}, m), 3051 (ν_{CH}, w), 1635 ($\nu_{C=N}$, s), 1578 ($\delta_{C=C}$, m), 1083 (ν_{ClO_4}, s), 626 (ν_{ClO_4}, s). Anal. found (calcd) for $C_{24}H_{32}Br_4ClFeN_4O_7$: C 32.15 (32.05); H 3.24 (3.59); N 6.80 (6.23).

2.4. Synthesis of compound **6** – [Fe(3,5-Br-salEen)$_2$]BPh$_4$·DMF

To a solution of *N*-ethylethylenediamine (0.105 mL, 1 mmol) in methanol (20 mL) 3,5-dibromosalicylaldehyde (279 mg, 1 mmol) was added and the yellow solution left stirring for 15 min. A solution of iron(II) chloride (64 mg, 0.5 mmol) and sodium tetraphenylborate (170 mg, 0.5 mmol) in methanol was added to the mixture and left stirring for 1 h. Filtration of the reaction mixture allowed to recover a dark microcrystalline solid. Recrystallisation from methanol/toluene/dimethylformamide (40:20:40) produced needle shaped crystals suitable for single crystal X-ray diffraction (250 mg, 23%). IR: ν_{max}/cm^{-1} 3210 (ν_{NH}, m), 3051 (ν_{CH}, w), 1633 ($\nu_{C=N}$, s), 1590 ($\delta_{C=C}$, m), 744 (ν_{BPh_4}, s), 708 (ν_{BPh_4}, s). Anal. found (calcd) for $C_{49}H_{53}BBr_4FeN_5O_3$: C 51.34 (51.34); H 4.78 (4.66); N 6.14 (6.11).

3. Results and discussion

3.1. Synthesis of complexes **1**–**6**

Complexes **1**–**6** were prepared as described in Scheme 1. The new complexes, **5** and **6** were obtained as solvated forms: [Fe(L$_C$)$_2$]ClO$_4$·EtOH (**5**) and [Fe(L$_C$)$_2$]BPh$_4$·DMF (**6**). In the solid state, crystalline samples of both complexes were characterised by elemental analysis, IR, ^{57}Mössbauer spectroscopy and SQUID magnetometry and the structure of complex **6** determined by single crystal X-ray diffraction. Solution properties of complexes **1**–**6** were determined at RT by UV–vis and NMR spectroscopies and their redox behaviour studied by cyclic voltammetry.

The IR spectrum of **5** presented a characteristic C=N stretching band at 1633 cm^{-1} and two ClO_4^- stretching bands at 1083 and 626 cm^{-1} confirming that formation of the imine was achieved and the exchange of the anion occurred. For complex **6** the IR spectrum also confirmed the success of the synthesis with stretching bands at 744 and 708 cm^{-1} attributed to BPh_4^- and 1633 cm^{-1} corresponding to the C=N group.

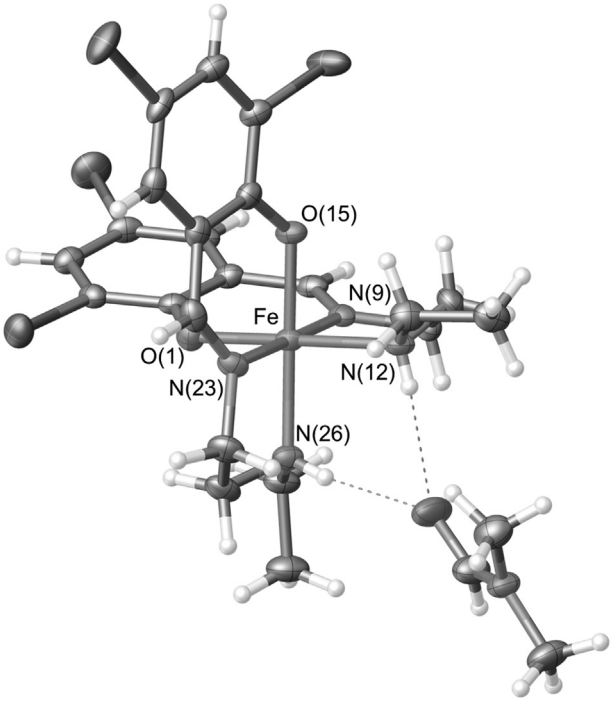

Fig. 1. ORTEP view of the association between [Fe(3,5-Br-salEen)$_2$]$^+$ and DMF with two N–H·O hydrogen bonds drawn as dashed lines and thermal ellipsoids drawn at the 50% probability level.

3.2. Crystal structure of compound **6**

The crystal structure of compound **6** is built up from an asymmetric unit composed of one cation [Fe(3,5-Br-salEen)$_2$]$^+$, one BPh_4^- anion and one DMF solvent molecule. The complex cation and DMF molecule are associated by two N–H···O hydrogen bonds with N···O distances of 2.962(3) and 2.928(3) Å and N–H···O angles of 170 and 172°, respectively. The ORTEP view of this association is presented in Fig. 1. The metal complex has a distorted octahedral geometry with three nitrogen atoms adopting a spatial disposition consistent with a *fac*-isomer. Selected bond distances and angles in the metal coordination sphere are listed in Table 2. The Fe–N (1.9279(2)–2.0315(2) Å) and Fe–O (1.8679(2) and 1.8765(2) Å) distances are consistent with the existence of a Fe(III) centre in the LS state and are equivalent to those observed for the analogous [Fe(5-Br-salEen)$_2$]BPh$_4$·DMF [40].

The crystal packing of **6** is view along the *b* crystallographic axis, shown in Fig. 2, and reveals that the BPh_4^- anions are arranged in

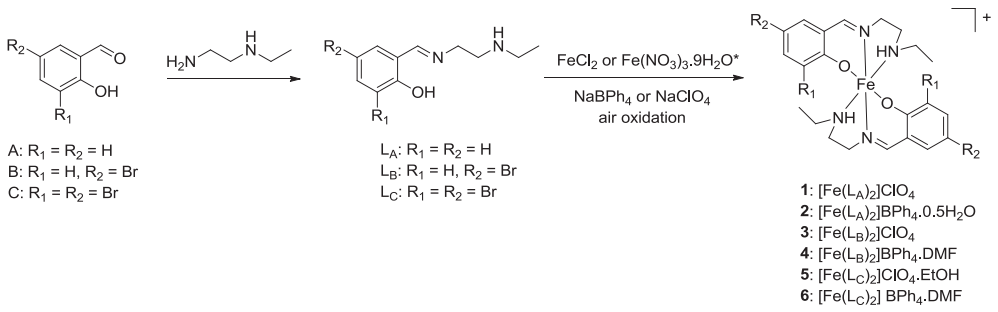

Scheme 1. General method used in the synthesis of complexes **1**–**6** (*for complexes **1**–**4**).

Table 2
Selected bond distances (Å) and angles (°) of **6**.

Bond lengths			
Fe–O(1)	1.8679(2)	Fe–N(12)	2.0283(2)
Fe–O(15)	1.8765(2)	Fe–N(23)	1.9222(2)
Fe–N(9)	1.9279(2)	Fe–N(26)	2.0315(2)
Bond angles			
O(1)–Fe–O(15)	94.25(8)	O(15)–Fe–N(26)	176.45(9)
O(1)–Fe–N(9)	93.38(8)	N(9)–Fe-N(12)	84.48(9)
O(1)–Fe–N(12)	177.27(9)	N(9)–Fe–N(23)	178.17(9)
O(1)–Fe–N(23)	86.85(8)	N(9)–Fe–N(26)	97.67(9)
O(1)–Fe–N(26)	86.81(9)	N(12)–Fe–N(23)	95.35(9)
O(15)–Fe–N(9)	85.65(9)	N(12)–Fe–N(26)	91.78(9)
O(15)–Fe–N(12)	87.29(9)	N(23)–Fe–N(26)	84.15(9)
O(15)–Fe–N(23)	92.52(8)		

the crystal in open channels, which accommodates the complex cations. The DMF crystallisation solvent molecules are positioned between BPh_4^- anions. The shortest intermolecular Fe···Fe distance is 8.991 Å indicating the absence of the electronic communication between the iron centres in the crystalline state.

3.3. Solid state characterisation of *5* and *6*

The magnetic profile of complexes **1** and **2** has been previously described [38,48]. While complex **1** showed thermal magnetic dependence exhibiting SCO behaviour, complex **2** is stabilised in the HS state over the measured temperature range. The thermal magnetic behaviour of crystalline samples **3**–**6** was measured by SQUID magnetometry on cooling and warming modes. Results obtained for complexes **3** and **4** are reported elsewhere [40], and indicated that although differently, both complexes exhibited incomplete SCO. Complex **3** showed a gradual SCO on cooling and an abrupt ST on warming with an asymmetric 70 K hysteresis loop. Compound **4** displayed a gradual SCO, and its magnetic behaviour showed to be sensitive to the applied magnetic field and sample thermal history.

Fig. 3 displays the results obtained for samples **5** and **6**. At low temperature both compounds are in the LS state with $\chi_m T$ values of 0.59 and 0.37 $cm^3\ mol^{-1}$ K, respectively. Complex **6** remains in the LS state up to 150 K, where $\chi_m T$ starts to increase slowly, displaying an incomplete thermal SCO, as indicated by the small value of $\chi_m T$, 2.4 $cm^3\ mol^{-1}$ K, obtained at the highest measured temperature, 370 K. In the case of complex **5** $\chi_m T$ values are almost constant (varying between 0.59 and 0.86 $cm^3\ mol^{-1}$ K), suggesting that the population of the LS state is essentially maintained up to 300 K.

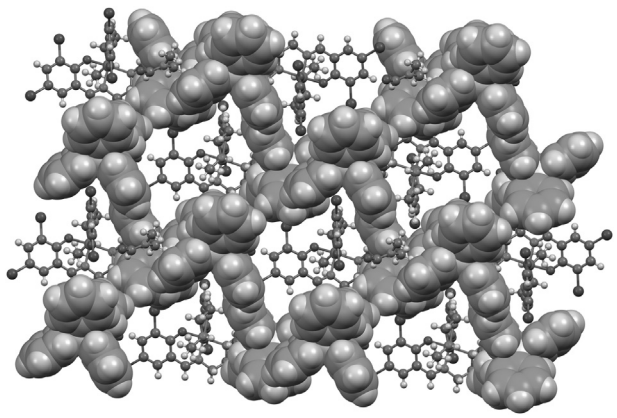

Fig. 2. Crystal packing diagram view along the *b* crystallographic axis showing the assembly of BPh_4^- anions in open channels, which are occupied by cations $[Fe(3,5\text{-}Br\text{-}salEen)_2]^+$. For clarity in each channel only one molecule of the complex is shown in ball-stick fashion. The BPh_4^- anions are represented in space filling mode.

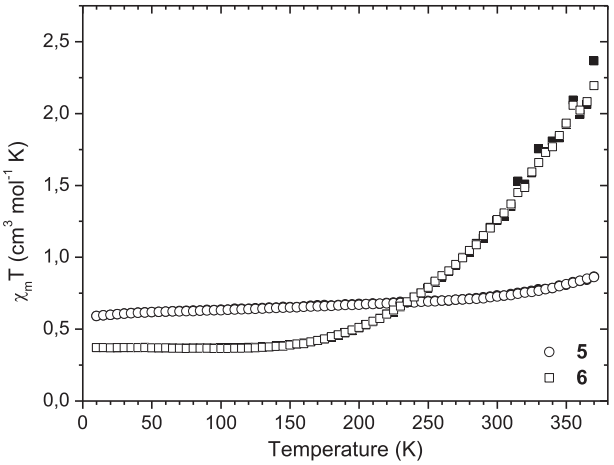

Fig. 3. Temperature dependence of $\chi_m T$ for compounds **5** and **6**, obtained under 1000 Oe, on cooling (solid symbols) and warming (open symbols).

Fig. 4 shows the Mössbauer spectra of complexes **5** (78 K and 290 K) and **6** (78 K), and the hyperfine parameters obtained from the fitting procedures are presented in Table 3. Mössbauer studies of compounds **3** and **4** are reported elsewhere [40].

The Mössbauer spectra collected at 78 K can be resolved using a single, but asymmetric, quadrupole doublet with isomer shifts (δ) around 0.2 mm/s and quadrupole splittings (ΔE_Q) near 2.8 mm/s, which are consistent with Fe(III) ions in an LS state. The assignment of this doublet to LS Fe(III) is also supported by the low temperature magnetisation results of both samples, with $\chi_m T$ values close to those expected for spin only $S = 1/2$, 0.38 $cm^3\ mol^{-1}$ K, particularly visible for compound **6**.

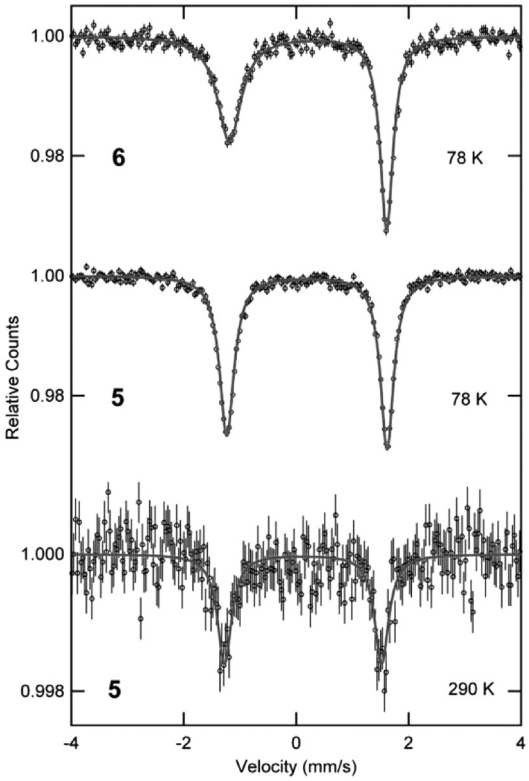

Fig. 4. ^{57}Fe Mössbauer spectra of complexes **5** (at 78 and 290 K) and **6** (at 78 K).

Table 3
Estimated parameters from the Mössbauer spectra of **5** and **6**.

290 K					78 K			
Compound	δ (mm/s)	ΔE_Q (mm/s)	Γ (mm/s)	W_{21} (mm/s)	δ (mm/s)	ΔE_Q (mm/s)	Γ (mm/s)	W_{21} (mm/s)
5	0.12(1)	2.80(2)	0.31(3)	–	0.191(1)	2.851(3)	0.312(5)	0.92(2)
6	0.20(5)	2.6(1)	0.9(2)	–	0.209(4)	2.798(7)	0.52(1)	0.54(1)

δ – isomer shift; ΔE_Q – quadrupole splitting; Γ – FWHM line width; W_{21} – relative line width.

At RT, the spectra of both complexes reveal poor resonant absorption due to the small fraction of recoilless iron nuclei. In fact one doublet is clearly perceptible in the RT spectrum of **5**, Fig. 4, agreeing with magnetisation data. The decrease observed in the isomer shift value compared to that obtained at 78 K can be explained by the second-order Doppler effect [3,49].

The RT spectrum resolution of **6** (not shown) is poor and it was not possible to clearly define the characteristics of two iron sites in a reasonable spectrum acquisition time, justifying the broad line width (Γ = 0.9(2) mm/s) and the mean isomer shift value (δ = 0.20(5) mm/s) obtained (Table 3). This is certainly due to a spin interconversion process running at 290 K, as shown by the magnetisation data (Fig. 3).

The asymmetric line broadening of the LS Fe(III) doublet observed for both complexes at 78 K, is estimated by parameter W_{21} (Table 3) which represents the relative line width between the higher and the lower energy absorption lines of the doublet. Both Fig. 4 and Table 3, clearly show that at 78 K this asymmetry is much more relevant for compound **6**, and the poor resolution of the RT spectra does not allow a meaningful quantification of W_{21} at this temperature. This type of line broadening asymmetry can be attributed to fluctuating electric and magnetic fields associated with the relaxation of paramagnetic ions, as well as to changes on the environment surrounding the iron nuclei [50]. Taking into account the slow but continuous spin interconversion of sample **6** above 100 K and the almost constant value of $\chi_m T$ for compound **5** (varying between 0.59 and 0.86 cm^3 mol^{-1} K), it is reasonable to accept that relaxation mechanisms associated with thermal SCO in compound **6** account for the high broad line asymmetry obtained.

3.4. Solution measurements

Complexes **1**–**6** were characterised by UV–vis spectroscopy and their redox behaviour studied by cyclic voltammetry. The magnetic susceptibility in solution of complexes **1**–**6** at RT was determined by the Evans' method [41] using ^{1}H NMR spectroscopy.

UV–vis spectra of compounds **1**–**6** were recorded at RT for solutions of each complex in acetonitrile (7×10^{-5} mol L^{-1}) and can be seen in Fig. 5.

The UV–vis spectra of all complexes display charge transfer and intraligand π–π^* transitions below 400 nm with ε varying between ≈4000 (**6**) and ≈12,000 mol L^{-1} cm^{-1} (**2**). For all six complexes, two additional absorbance bands appear in the region 450–850 nm possibly from the ligand-to-metal charge transfer (LMCT) transitions, Table 4. Electronic studies on Fe(III) complexes bearing (sal)$_2$trien (trien = triethylenetetramine) ligands showed that in the 450–850 nm region there is a higher energy band corresponding to the HS species and a second band at lower energy assigned to the LS species [51]. Taking this into account, we attribute the bands between 519 nm < λ_{max} < 548 nm to the HS species and those between 655 nm < λ_{max} < 680 nm to the LS species.

For complexes **1**–**6** the band attributed to the HS species shows a pronounced difference directly related to the degree of substitution at the phenolate ring. The non-substituted compounds (**1** and **2**) present the maximum absorbance at higher energy (519 nm for **1** and 520 nm for **2**). This is followed by the compounds bearing ligands with one electron withdrawing group (5-Br-salEen), **3** and **4**, exhibiting the maximum absorbance at 534 nm. Finally, the introduction of a second electron withdrawing group at the phenolate ring (3,5-Br-salEen) shifted the absorption maxima to lower energies (558 nm for **5** and 548 nm for **6**). It is worth noticing that the presence of either one or two electron withdrawing groups at the phenolate ring causes a red shift. Bromine, with σ-inductive electron withdrawing character, restricts the electron density available. This restriction alters the ligand field as well as the Δ_{oct} and, according to Tweedle and Wilson, such changes should be more pronounced for substituents *ortho* to the oxygen atom at the phenolate ring [51]. In fact the electronic spectra of complexes **1**–**6** at RT show this effect. The difference between the ε values of the HS and LS bands is smaller for complexes **5** and **6** when compared to those of complexes **1**–**4** indicating a clear effect of the phenolate substitution on the spin equilibrium.

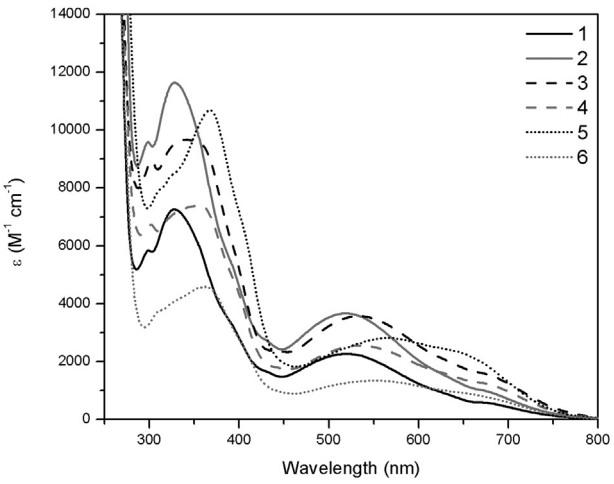

Fig. 5. RT UV–vis spectra of complexes **1**–**6** for 7×10^{-5} mol L^{-1} acetonitrile solutions.

Magnetic susceptibilities of all complexes at RT were determined using the Evans' method [41] where the RT ^{1}H NMR spectra of 5 mM solutions of **1**–**6** in CD_3CN with 0.03% TMS were recorded against a reference solution of 0.03% TMS in CD_3CN, Table 4. The $\chi_m T$ value of complex **1** (4.41 cm^3 mol^{-1} K) shows that this complex

Table 4
Electronic absorption maxima and extinction coefficients in acetonitrile and $\chi_m T$ values obtained from ^{1}H NMR results in CD_3CN for **1**–**6** at RT.

	ClO_4^-			BPh_4^-		
	R_1 = H, R_2 = H	R_1 = H, R_2 = Br	R_1 = Br, R_2 = Br	R_1 = H, R_2 = H	R_1 = H, R_2 = Br	R_1 = Br, R_2 = Br
	1	**3**	**5**	**2**	**4**	**6**
λ_{max} (nm)	519	534	558	520	534	548
ε (mol L^{-1} cm^{-1})	2271	3571	2806	3670	2556	1343
λ_{max} (nm)	678	678	655	678	680	673
ε (mol L^{-1} cm^{-1})	569	1547	2227	959	1206	797
$\chi_m T$ (cm^3 mol^{-1} K)	4.4	2.7	1.6	3.1	3.1	2.0

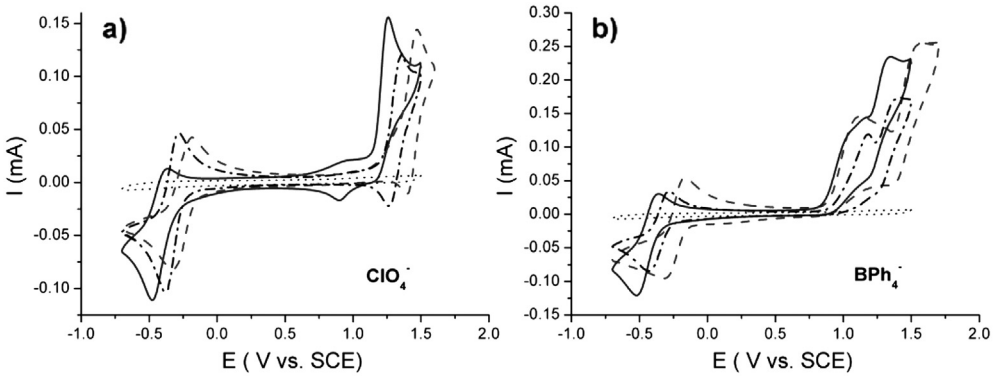

Fig. 6. Cyclic voltammograms of a Pt electrode in acetonitrile solutions with 0.1 M of NBu_4BF_4 as supporting electrolyte containing 1 mM of a) complexes **1** (solid line), **3** (dash dotted line) and **5** (dashed line) and b) complexes **2** (solid line), **4** (dash dotted line) and **6** (dashed line). Cyclic voltammogram of 0.1 M of NBu_4BF_4 in acetonitrile (dotted line). Scan rate: 200 mV s^{-1}.

is essentially in the HS state at RT, while the values obtained for all the other complexes indicate a mixture of both HS and LS states. Complexes **5** and **6**, for which $R_1 = R_2 = Br$, are those exhibiting the lowest $\chi_m T$ values, indicating a major fraction of LS state at RT. For complexes **2**, **3** and **4** the $\chi_m T$ values indicate a major fraction of HS state, with values of 67, 59 and 69% respectively. These results clearly show the ligand influence on the magnetic behaviour of the metal in solution, as the $\chi_m T$ value, and thus of HS fraction, decreases with the presence of bromide substituents at the phenolate ring. This fact is observed for the three complexes containing ClO_4^- and also for the solvated complexes **4** and **6** (BPh_4^- as anion). Within the same ligand, a variation of $\chi_m T$ is also observed when solvates are present and the anion changes. These observations indicate that the solvent and/or anion interact with the complex cation, affecting the $\chi_m T$ value.

These results are in good agreement with those of the UV–vis measurements confirming that the second bromide at the phenolate ring has an effect on the ligand field strength increasing the separation between the t_{2g} and the e_g^* energy levels. Further work is now underway to investigate the solvent and temperature effect on the magnetic behaviour of these complexes.

The redox behaviour of complexes **1**–**6** in acetonitrile was determined at RT by cyclic voltammetry (Fig. 6). Well-defined anodic and cathodic peaks with $E_{1/2}$ values between −0.441 and −0.225 V (Table 5) are related to the iron centres. Additionally, complexes **2**, **4** and **6** show peaks between 0.750 and 1.7 V that can be related to redox processes of both ligands and BPh_4^-. Within the same potential range complexes **1**, **3** and **5** only display ligand related redox processes, as the ClO_4^- anion did not show a redox response in the potential range studied. Attempts to isolate the ligands in order to clarify their redox processes were unsuccessful.

The fact that the electrochemical behaviour of the complexes is affected by the number of electron withdrawing groups at the phenolate ring is noteworthy. Namely, all redox processes shift to more positive values with the increase of bromide substituents at the ring, Fig. 6. This fact is clearly perceptible when the $E_{1/2}$ values of the iron redox processes (Table 5) are compared: a value of $E_{1/2} = -0.414$ V is observed for complex **1**, and the presence of one bromide substituent at the phenolate ring (complex **3**) shifts this value by 100 mV to more positive values (−0.310 V). Additionally an even higher shift to positive values (−0.250 V) is observed when a second bromide (complex **5**) is present at the ligand. This trend is also observed for the BPh_4^- complexes **2**, **4** and **6**. These results demonstrate that the reduction of the iron centre is easier with the increase of bromide substituents at the ring. However, the nature of the anion (ClO_4^- or BPh_4^-) does not significantly affect the $E_{1/2}$ values of the iron centres, Table 5. While complex **1** exhibits a reversible redox process ($\Delta E_p = 59$ mV) all other complexes show a quasi-reversible behaviour ($\Delta E_p > 59$ mV) [52].

Table 5
Electrochemical data of complexes **1**–**6**.[a]

Complex			$E_{Fe(III)/Fe(II)}$/V	$E_{Fe(II)/Fe(III)}$/V	$E_{1/2}$/V	ΔE_p/V
ClO_4^-	**1**	$R_1 = R_2 = H$	−0.478	−0.360	−0.414	0.059
	3 [40]	$R_2 = Br$	−0.360	−0.260	−0.310	0.100
	5	$R_1 = R_2 = Br$	−0.325	−0.185	−0.250	0.070
BPh_4^-	**2**	$R_1 = R_2 = H$	−0.515	−0.357	−0.441	0.079
	4 [40]	$R_2 = Br$	−0.350	−0.280	−0.320	0.070
	6	$R_1 = R_2 = Br$	−0.300	−0.160	−0.225	0.070

[a] Acetonitrile solution, 0.1 M NBu_4BF_4 as supporting electrolyte: $E_{1/2}$ vs. SCE, Pt working electrode, $\nu = 200$ mV s^{-1} Fc^+/Fc ($E_{1/2} = +0.420$ V [42]) as internal standard. $E_{1/2} = ½ (E_{pa} + E_{pc})$, $\Delta E_p = E_{pa} - E_{pc}$ (mV).

The redox processes of the ligands analysed by the results obtained for ClO_4^- complexes (**1**, **3** and **5**, Fig. 6a), show a shift to more positive values with the increase of bromide substituents at the phenolate ring. This can be attributed to the presence of electron withdrawing groups at the ring, restricting the electron density available at the ligand. For the BPh_4^- complexes (**2**, **4** and **6**, Fig. 6b) it has to be noted that the anion itself can also be oxidised over the same potential window as the ligand (Fig. S1 of the Supporting information), challenging the clear identification of the processes involving both ligand and anion.

4. Conclusions

Two new complexes, $[Fe(3,5\text{-Br-salEen})_2]ClO_4 \cdot EtOH$ (**5**) and $[Fe(3,5\text{-Br-salEen})_2]BPh_4 \cdot DMF$ (**6**) were synthesised and their magnetic properties investigated. The crystal packing diagram of complex **6** showed that the interaction between the metal centres is obstructed by the anion, affecting the SCO behaviour. SQUID magnetometry and Mössbauer spectroscopy showed that while **6** presents a gradual and incomplete SCO, **5** stabilises in the LS state up to 300 K. Comparison of the solid state magnetic profiles of newly reported complexes **5** and **6** with previously reported complexes **1**–**4** did not allow to draw conclusions on the influence of ligand substituent (σ-inductive electron withdrawing groups − bromine) on their magnetic behaviour. However, both spectroscopic and electrochemical studies of the complexes in solution have shown that there is a clear effect on their properties depending on the degree of substitution at the phenolate ring. Interestingly, both UV–vis measurements and Evans magnetic

susceptibility determinations at concentrations separated by a factor of ≈100 (0.07 mM for UV–vis and 5 mM for Evans' method) confirmed the effect of the ligand substituents on their magnetic character. The results indicate that in solution complex **1** is essentially in the HS state, and both HS and LS forms are present for the other complexes. When compared to the unsubstituted complexes (**1** and **2**), a significant decrease on $\chi_m T$ is observed when two bromide substituents are present at the phenolate ring, showing a clear preference for the LS state, and indicating an increased separation between the t_{2g} and e_g^* energy levels. The bromide substituent effect has also been observed on the electrochemical behaviour of the complexes. The reduction of the metallic centres proved to be easier for ligands with increasing number of electron withdrawing groups, as the $E_{1/2}$ values of iron shift to more positive potentials.

Acknowledgements

We thank Fundação para Ciência e Tecnologia for financial support (PEst-OE/QUI/UI0612/2013, PEst-OE/QUI/UI0536/2011, PEst-OE/FIS/UI0261/2011 and PTDC/QUI-QUI/101022/2008) and fellowships to AIM (SFRH/BPD/69526/2010), PNM (SFRH/BPD/73345/2010), MSS (SFRH/BPD/88082/2012).

Appendix A. Supplementary material

CCDC 976390 contains the supplementary crystallographic data for this paper. These data can be obtained free of charge from The Cambridge Crystallographic Data Centre via www.ccdc.cam.ac.uk/data_request/cif.

Appendix B. Supplementary information

Supplementary data related to this article can be found at http://dx.doi.org/10.1016/j.jorganchem.2013.12.028.

References

[1] P.A. Vigato, S. Tamburini, Coord. Chem. Rev. 248 (2004) 1717–2128.
[2] H. Toftlund, J.J. McGarvey, Top. Curr. Chem. 233 (2004) 151–166.
[3] P.J. van Koningsbruggen, Y. Maeda, H. Oshio, Top. Curr. Chem. 233 (2004) 259–324.
[4] P. Gutlich, H.A. Goodwin, Top. Curr. Chem. 233 (2004) 1–47.
[5] L. Cambi, L. Szegö, Ber. Dtsch. Chem. Ges. 64 (1931) 2591–2598.
[6] L. Cambi, L. Szegö, Ber. Dtsch. Chem. Ges. 66 (1933) 656–661.
[7] L. Cambi, L. Malatesta, Ber. Dtsch. Chem. Ges. 70 (1937) 2067–2078.
[8] O. Kahn, E. Codjovi, Y. Garcia, P.J. van Koningsbruggen, R. Lapouyade, L. Sommier, ACS Sym. Ser. 644 (1996) 298–310.
[9] P. Gutlich, P.J. van Koningsbruggen, F. Renz, Struct. Bond. 107 (2004) 27–75.
[10] H.A. Goodwin, Top. Curr. Chem. 234 (2004) 23–47.
[11] Y. Garcia, P. Gutlich, Top. Curr. Chem. 234 (2004) 49–62.
[12] A. Hauser, Top. Curr. Chem. 233 (2004) 49–58.
[13] M.A. Halcrow, Spin-crossover Materials: Properties and Applications, John Wiley & Sons Ltd, 2013.
[14] S.B. Erenburg, N.V. Bausk, L.G. Lavrenova, V.A. Varnek, L.N. Mazalov, Solid State Ionics 101 (1997) 571–577.
[15] Y. Garcia, P.J. van Koningsbruggen, R. Lapouyade, L. Fournes, L. Rabardel, O. Kahn, V. Ksenofontov, G. Levchenko, P. Gutlich, Chem. Mater. 10 (1998) 2426–2433.
[16] Y. Garcia, V. Niel, M.C. Munoz, J.A. Real, Top. Curr. Chem. 233 (2004) 229–257.
[17] M. Ruben, U. Ziener, J.M. Lehn, V. Ksenofontov, P. Gutlich, G.B.M. Vaughan, Chem. Eur. J. 11 (2004) 94–100.
[18] T. Kitazawa, Y. Gomi, M. Takahashi, M. Takeda, M. Enomoto, A. Miyazaki, T. Enoki, J. Mater. Chem. 6 (1996) 119–121.
[19] V. Niel, J.M. Martinez-Agudo, M.C. Munoz, A.B. Gaspar, J.A. Real, Inorg. Chem. 40 (2001) 3838.
[20] O. Roubeau, A. Colin, W. Schmitt, R. Clerac, Angew. Chem. Int. Ed. 43 (2004) 3283–3286.
[21] P. Grondin, O. Roubeau, M. Castro, H. Saadaoui, A. Colin, R. Clerac, Langmuir 26 (2010) 5184–5195.
[22] T. Fujigaya, D.L. Jiang, T. Aida, Chem. Asian J. 2 (2007) 106–113.
[23] Y. Galyametdinov, V. Ksenofontov, A. Prosvirin, I. Ovchinnikov, G. Ivanova, P. Gütlich, W. Haase, Angew. Chem. Int. Ed. 40 (2001) 4269–4271.
[24] Y. Bodenthin, G. Schwarz, Z. Tomkowicz, M. Lommel, T. Geue, W. Haase, H. Mohwald, U. Pietsch, D.G. Kurth, Coord. Chem. Rev. 253 (2009) 2414–2422.
[25] A.B. Gaspar, M. Seredyuk, R. Gutlich, Coord. Chem. Rev. 253 (2009) 2399–2413.
[26] E. Coronado, J.R. Galan-Mascaros, M. Monrabal-Capilla, J. Garcia-Martinez, P. Pardo-Ibanez, Adv. Mater. 19 (2007) 1359.
[27] T. Forestier, S. Mornet, N. Daro, T. Nishihara, S. Mouri, K. Tanaka, O. Fouche, E. Freysz, J.F. Letard, Chem. Commun. (2008) 4327–4329.
[28] F. Volatron, L. Catala, E. Riviere, A. Gloter, O. Stephan, T. Mallah, Inorg. Chem. 47 (2008) 6584–6586.
[29] I. Boldog, A.B. Gaspar, V. Martinez, P. Pardo-Ibanez, V. Ksenofontov, A. Bhattacharjee, P. Gutlich, J.A. Real, Angew. Chem. Int. Ed. 47 (2008) 6433–6437.
[30] P.N. Martinho, T. Lemma, B. Gildea, G. Picardi, H. Muller-Bunz, R.J. Forster, T.E. Keyes, G. Redmond, G.G. Morgan, Angew. Chem. Int. Ed. 51 (2012) 11995–11999.
[31] A. Ruaudelteixier, A. Barraud, P. Coronel, O. Kahn, Thin Solid Films 160 (1988) 107–115.
[32] P. Coronel, A. Barraud, R. Claude, O. Kahn, A. Ruaudelteixier, J. Zarembowitch, J. Chem. Soc. Chem. Commun. (1989) 193–194.
[33] S. Cobo, G. Molnar, J.A. Real, A. Bousseksou, Angew. Chem. Int. Ed. 45 (2006) 5786–5789.
[34] M. Cavallini, I. Bergenti, S. Milita, G. Ruani, I. Salitros, Z.R. Qu, R. Chandrasekar, M. Ruben, Angew. Chem. Int. Ed. 47 (2008) 8596–8600.
[35] M.S. Haddad, M.W. Lynch, W.D. Federer, D.N. Hendrickson, Inorg. Chem. 20 (1981) 123–131.
[36] M.S. Haddad, W.D. Federer, M.W. Lynch, D.N. Hendrickson, J. Am. Chem. Soc. 102 (1980) 1468–1470.
[37] T.A. Ivanova, I.V. Ovchinnikov, A.N. Turanov, Phys. Solid State 49 (2007) 2132–2137.
[38] M.S. Haddad, W.D. Federer, M.W. Lynch, D.N. Hendrickson, Inorg. Chem. 20 (1981) 131–139.
[39] P.N. Martinho, Y. Ortin, B. Gildea, C. Gandolfi, G. McKerr, B. O'Hagan, M. Albrecht, G.G. Morgan, Dalton Trans. 41 (2012) 7461–7463.
[40] A.I. Vicente, S. Realista, L.P. Ferreira, M.D. Carvalho, A. Melato, P. Brandão, M.J. Calhorda, P.N. Martinho, (2013), submitted for publication.
[41] D.F. Evans, J. Chem. Soc. (1959) 2003–2005.
[42] M.A. Vorotyntsev, M. Casalta, E. Pousson, L. Roullier, G. Boni, C. Moise, Electrochim. Acta 46 (2001) 4017–4033.
[43] Bruker, SAINT-plus, Bruker AXS Inc, Madison, Wisconsin, USA, 2007.
[44] G.M. Sheldrick, SADABS, University of Göttingen, Germany, 1996.
[45] G.M. Sheldrick, Acta Crystallogr. A64 (2008) 112.
[46] O.V. Dolomanov, L.J. Bourhis, R.J. Gildea, J.A.K. Howard, H. Puschmann, J. Appl. Crystallogr. 42 (2009) 339–341.
[47] C.F. Macrae, I.J. Bruno, J.A. Chisholm, P.R. Edgington, P. McCabe, E. Pidcock, L. Rodriguez-Monge, R. Taylor, J. van de Streek, P.A. Wood, Appl. Crystallogr. 41 (2008) 466–470.
[48] C.F. Sheu, S.M. Chen, G.H. Lee, Y.H. Liu, Y.S. Wen, J.J. Lee, Y.C. Chuang, Y. Wang, Eur. J. Inorg. Chem. (2013) 894–901.
[49] P. Gütlich, E. Bill, A.X. Trautwein, Mössbauer Spectroscopy and Transition Metal Chemistry, Springer-Verlag, Berlin, Heidelberg, 2011.
[50] M. Blume, Phys. Rev. Lett. 14 (1965) 96–98.
[51] M.F. Tweedle, L.J. Wilson, J. Am. Chem. Soc. 98 (1976) 4824–4834.
[52] D. Pletcher, R. Greff, R. Peat, L.M. Peter, J. Robinson, Instrumental Methods in Electrochemistry, Ellis Horwood Ltd, 1990.